# Connectivity of Hydrogen Bond Networks in EDL Dominates the Kinetical pH Effect of Hydrogen Electrocatalysis on Pt

**Peng Li**
Wuhan University
**Yaling Jiang**
College of Chemistry and Molecular Sciences, Wuhan University
**Youcheng Hu**
College of Chemistry and Molecular Sciences, Wuhan University
**Yana Men**
Wuhan University
**Yuwen Liu**
College of Chemistry and Molecular Sciences, Wuhan University
**Wenbin Cai**
Fudan University
**Shengli Chen** ( slchen@whu.edu.cn )
College of Chemistry and Molecular Sciences, Wuhan University https://orcid.org/0000-0001-7448-8860

**Article**

**Keywords:**

**Posted Date:** February 24th, 2022

**DOI:** https://doi.org/10.21203/rs.3.rs-1344825/v1



**Version of Record:** A version of this preprint was published at Nature Catalysis on September 29th, 2022.
See the published version at https://doi.org/10.1038/s41929-022-00846-8.

# Abstract

The hydrogen evolution reaction (HER) on Pt and other noble metals often undergo ~2 orders of magnitude decrease in reaction kinetics when changing the electrolyte pH from acid to alkaline regime. The origin of this kinetic pH effect remains far from a consensus, hindering the rational design of pH-specific electrocatalysts. Herein, by meticulously comparing the electric double layer (EDL) structures of acid and alkaline interfaces from the *ab initio* molecular dynamics (AIMD) simulations, and the computational vibration spectra of water molecules in the AIMD-simulated interfaces with the results of *in situ* surface-enhanced infrared absorption spectroscopy (SEIRAS), we conclude that neither the hydrogen adsorption strength nor the water dissociation barrier is responsible for the greatly reduced HER kinetics on Pt in alkaline media, because the alkaline interface could have more favorite hydrogen adsorption strength and lower barriers for individual Volmer reactions; it is the significantly different connectivity of hydrogen bond networks in EDL that cause the huge kinetic pH effect of HER. What's further, using Pt-Ru alloy as model, our results reveal an unprecedented role of OH adsorption in improving the kinetics of alkaline hydrogen electrocatalysis on Pt-based catalysts, namely, by increasing the connectivity of hydrogen bond networks in EDL rather than by directly affecting the energetics of surface steps. These findings should add significant new insights into the key roles of EDL structures in electrocatalysis. Meanwhile, this study offers a referential research paradigm for exploring the atomic structures of electrochemical interfaces by combining AIMD simulations, computational spectroscopy, and experimental spectroscopy.


# Introduction

Due to its high mass energy density and carbon-free nature, hydrogen is considered the most promising energy carrier of the future[1–4]. The hydrogen evolution reaction (HER) and hydrogen oxidation reaction (HOR) are the footstones of the hydrogen energy. Besides their technological importance in water electrolysis and fuel cells, the HER/HOR have long served as the model reactions in electrochemistry due to the relatively simple reaction mechanism[5–8]. A standing puzzle in the fundamental chemistry of hydrogen electrocatalysis is the origin of the orders of magnitude decrease in reaction kinetics when moving from acid to alkaline, which has seriously retarded the further development of alkaline electrolysis and fuel cells and has attracted great recent research interest [9–13].

So far, there are several schools-of-thought to explain the kinetically sluggish HER/HOR process in alkaline environment. Yan and co-workers attributed it to the pH-dependent hydrogen binding energy (HBE)[14,15]. They found that the HBE, inferred from the potential of underpotential-deposited hydrogen ($H_{upd}$) peaks in cyclic voltammograms, linearly increase with the pH, while the experimental HER/HOR activity decreases with the pH. On this basis, the HBE has been proposed to be the sole descriptor for the HER/HOR activity. Recently, a modified HBE theory has been proposed that the apparent hydrogen binding energy ($HBE_{app}$), the adsorption strength difference between H and water on electrocatalyst surface, determines the HER/HOR activity[16–18]. However, it was also argued that the shift of voltametric

peak for $H_{upd}$ is due to the change in the hydroxyl adsorption strength[19–20]. Additionally, the HBE theory cannot explain the great pH-dependence of HER/HOR kinetics on Pt(111) surface, at which the voltammetric peak for $H_{upd}$ hardly shifts with pH[21]. What's more, the results from *in situ* surface-enhanced infrared adsorption spectroscopy (SEIRAS) and Raman (SERS) spectroscopy have indicated that the H binding strength becomes monotonously weakened as the pH increases, which significantly challenges the foundation of the HBE theory[22,23].

Another prevailing school-of-thought suggests that the high activation barrier of alkaline Volmer step ($H_2O + e^- \leftrightarrow *H + OH^-$) derived from the cleavage/formation of H-OH bond is the origin of the pH effect on HER/HOR kinetics[10,24]. By contrast, the hydronium ions as the proton donors in acid environment implies an unobstructed Volmer step ($H_3O^+ + e^- \leftrightarrow *H + H_2O$). Markovic and co-workers reported that the combination of Pt with components having high oxophilicity, such as hydroxides, oxides and Ru et al., can distinctly promote the dissociation of water and/or the adsorption of hydroxyl species, thereby yielding higher HER/HOR kinetics in alkaline environment[25–27]. The so-called bifunctional mechanism thus proposed has been widely used nowadays to guide the design of high-efficient alkaline HER/HOR electrocatalysts[28,29]. However, this view was questioned by some results which imply that the electronic effect of Ru is responsible for the enhanced hydrogen reaction kinetics at high pH[11,30]. Meanwhile, the role of hydroxyl species ($OH^-$ or $OH_{ad}$) in alkaline hydrogen electrocatalysis are still elusive and under extensive debates[31–35].

The pH-dependent kinetics of HER/HOR has also been attributed to the varied interfacial environment with pH. Koper and co-workers contended that the great deviation of the electrode potential from the potential of zero charge (PZC) leads to a strong interfacial electrical field, which significantly increases the water-reorganization energy, and thus impedes the proton/hydroxide transfer across the electrical double layer (EDL)[21,36]. Following this idea, the pH-dependent kinetics on Pt(111) electrode and the activity improvement of alkaline hydrogen electrocatalytic reactions by introducing $Ni(OH)_2$ on Pt also can be explained in terms of interfacial rigidity associated with PZC. The roles of EDL factors, for examples, the electrostatic interactions and dynamics of interfacial water molecules, in the pH-dependent kinetics hydrogen electrocatalytic kinetics has also been highlighted by other researchers[37,38]. In addition, it has recently been proposed by some researchers that the interfacial hydrogen bond (H-bond) networks may play a critical role in the kinetics of interfacial proton-coupled electron transfer (PCET) reactions[39–41]. So far, these EDL propositions remain lacking atomic/molecular-level evidences.

In this study, taking the HER on Pt(111) surface as the model system, the underlying origin of the pH-dependent reaction kinetics is investigated by combining *ab initio* molecular dynamics (AIMD) simulation and *in situ* surface-enhanced infrared absorption spectroscopy (SEIRAS) with the attenuated total reflection (ATR) configuration. The AIMD simulation results imply that neither the hydrogen adsorption strength nor the water dissociation barrier is responsible for the greatly reduced kinetics of hydrogen electrocatalysis in alkaline solution. Interestingly, by carefully analyzing the AIMD-simulated EDL

structures, we notice that there exists a visible gap of water at alkaline interface, which should result in greatly reduced connectivity of hydrogen bond networks and therefore increased hydrogen transfer barrier in interfacial region. More importantly, the simulated interfacial structures are unequivocally verified by the agreements between the computational vibrational spectra and the experiment SEIRAS results. What's further, the AIMD simulations for Pt-Ru alloy show that the adsorbed OH ($OH_{ad}$) species on Ru site can significantly improve the connectivity of hydrogen bond networks at alkaline interface. This unprecedented role of $OH_{ad}$ explains well why PtRu is much more active than Pt for hydrogen electrocatalytic reactions in alkaline, and further confirms the critical role of interfacial hydrogen bond connectivity in the HER/HOR kinetics. These findings should add new insights into the critical role of interfacial EDL in electrocatalytic kinetics, and provide a novel perspective to understand the electrocatalytic pH effects which are of general significance in various energy conversion reactions such as HER/HOR, $CO_2$ reduction and nitrogen reduction. Meanwhile, this study also offers a referable research paradigm for exploring the microstructure and process at the electrochemical interfaces by combining the AIMD simulations, computational spectroscopy, and experimental spectroscopy.

# Results

**EDL structures of acid and alkaline interfaces at HER potentials.** It is found that, for the interface models with a 4·4 orthogonal Pt(111) slab used in present study (Supplementary Figs. 1-3), the introduction of two $H_3O^+$ and four $Na^+$ cations respectively into the water layers, and the same number of electrons into the electrode accordingly, can drive the electrode potentials (U) to values corresponding to the HER potentials for acid and alkaline systems, that are, ca. -0.20 V for pH=0 and ca. -0.32 V for pH=14 (unless stated, potentials in this paper are referenced to the reversible hydrogen electrode, RHE). The much higher electron density on electrode surface for the alkaline system is easy to understand when considering that the HER potentials are much further away from the potential of zero charge (PZC). As stated in the Methods section, the co-ions and the Gouy-Chapman diffusion layer can be neglected in the strong acid and alkaline systems. Therefore, we focus on the differences between the EDL structures at acid and alkaline interfaces associated with the profiles of cations. Figure 1a,b show the representative AIMD snapshots for the acid and alkaline interfaces, respectively. The statistic concentration profiles and trajectory analyses of $H_3O^+$ and $Na^+$ distinctly demonstrate a layered distribution of cation in both acid and alkaline EDL (Supplementary Fig. 4).

The cations closest to the electrode surface constitute the outer Helmholtz planes (OHPs), which are at distances of ~4.26 Å and ~2.92 Å away from the electrode surface for acid and alkaline systems, respectively. The alkaline OHP bears much higher ion concentration than the acid one. The crowded cations at alkaline OHP lose considerably their solvation molecules, which can be seen from the Na-O radial distribution functions ($g_{Na-O}$) shown in Supplementary Fig. 5. In addition, there hardly see water molecules within the alkaline OHP. At acid interface, in contrast, the protons are well solvated and the OHP is separated from the electrode surface by water molecules. Such differences between the cation and water distributions in the acid and alkaline EDLs should be ascribed to the much higher negative

charge density of electrode surface at alkaline interface and higher mobility of protons. The position of the OHP in alkaline media agrees well with that measured through the surface X-ray scattering technology[42,43], which rationalizes our simulated EDL structures.

The interfacial distributions of water molecules, represented by the oxygen concentration profiles along the surface normal direction, are further illustrated (Fig. 1c). It is apparent that at the distance of ~3.30 Å away from the Pt surface, both acid and alkaline interfaces exhibit a sharp peak of oxygen concentration, which is within the acid OHP while out of the alkaline OHP, again suggesting that there no water molecules being present between the cations and electrode surface at alkaline interface. As marked by the shadow, both the acid and alkaline interfaces possess a “gap zone” above the OHP, in which the water concentration is fairly low, and beyond which the water concentration fluctuates around the bulk value (0.056 mol/cm$^3$). The “gap zone” at alkaline interface is apparently larger in width and more depleted in water concentration than that at acid interface. It is imaginable that the severe depletion of water molecule would reduce the connectivity of the H-bond networks at alkaline interface, which is verified by the statistical distributions of H-bond number along the surface normal direction (Fig. 1d). It is seen that there exists a region around ~4.2 Å away from the Pt surface (orange shadow) at alkaline interface, in which the H-bond number is significantly diminished as compared with the neighboring regions. Such diminishment in H-bond should be due to the large decrease in the numbers of solvated water molecules of the crowed OHP cations and the strong interaction between the OHP cations and their solvated water molecules, which significantly reduce the ability of these water molecules to form H-bond with others. It is conceivable that the greatly reduced connectivity of H-bond networks near the electrode surface would severely inhibit the hydrogen electrocatalytic reactions, since the H-bond networks constitute highways for delivering proton to surface, which, as will be shown in the following, is vital in hydrogen electrocatalysis. On the contrary, the H-bond number at acid interface is with little contrast to that in the bulk region.

**Origin of the greatly different HER kinetics at acid and alkaline interfaces.** The HER essentially involves hydrogen transfer (HT) processes, via the Volmer and/or Heyrovsky reaction. It has been argued that the great difference between the HER kinetics at acid and alkaline interfaces is due to the different hydrogen sources, namely, hydroniums ($H_3O^+$) at acid interface and water molecules at alkaline interface. The HT through water dissociation is traditionally believed to have high energy barrier than that through $H_3O^+$. As implied in the simulated EDL structures (Fig. 1a,b), the closest hydroniums ($H_3O^+$) at acid interface are separated from electrode surface by interfacial water molecules. Therefore, it should be the water molecules closely neighboring the electrode surface rather than the $H_3O^+$ that directly participate the HT processes in acid HER. Thus, the HER kinetics at acid and alkaline interfaces may be compared by investigating the HT processes of the water molecules closest to electrode surface. We consider the Volmer reaction for simplicity. The slow-growth method is used to evaluate the free energy barriers ($\Delta G^{\neq}$) of the individual Volmer reaction, with each closest water molecule serving as the direct dissociative reactant to form $H_{ad}$ (Supplementary Fig. 6). At acid interface, the collective variable (CV) is defined as

the combination of several O-H distances connecting the hydrogen bond networks from $H_3O^+$ to closet water molecule, while the O-H bond length of interface water molecule is directly used as the CV in alkaline media (Supplementary Fig. 7). To ensure the accuracy and reliability of the free energy barriers comparison, the slow-growth simulation for each water molecule has been performed three times independently to obtain the error analysis. In acid Volmer reactions, the hydronium at OHP transfers H to the dissociated water molecules closet to the electrode surface through the H-bond networks in the EDL (Supplementary Fig. 8); while in alkaline, the dissociated water molecules closest to the surface gains H through the H-bond networks in the EDL and meanwhile a hydroxyl anion ($OH^-$) is produced in the region out of OHP (Supplementary Fig. 9). As illustrated in Fig. 2a, surprisingly, the Volmer reactions of various water molecules at the acid interface have higher free energy barriers than those at the alkaline interface, which contradicts the long-established belief that the alkaline HT processes should be more energy-demanding than the acid ones through the dissociation of interfacial hydronium[26]. When considering the EDL structures, however, the lower free energy barrier of individual HT process in alkaline becomes reasonable.

As having been mentioned above, it is the water molecules closely neighboring the electrode surface rather than the $H_3O^+$ cations that directly act as the HT sources to form $H_{ad}$ at acid interface. Therefore, the energy-limiting step of the HT processes at both the acid and alkaline interfaces should be the dissociation of the closest water molecules. At alkaline interface, these water molecules are strongly polarized by cations, which will significantly weaken the O-H bond strength and thereby lower the dissociation barrier. The facilitated reactivity by the interacting metal cations has been corroborated experimentally[44]. In addition, the electrode surface with much higher negative charge density should strongly attract the hydrogen atoms in water, which further facilitates the breakage of O-H bond of the nearby water molecules. Consequently, the ~2 orders of magnitude lowering in the alkaline HER activity cannot be simply attributed to the change of H source from hydronium ions to water molecules.

Besides the dissociation of the closest water molecules, the HT through the H-bond networks in EDL is also essentially involved in the HER process. As revealed in the simulated EDL structures (Fig. 1d), the H-bond number is significantly diminished in the region near alkaline OHP. The scarcity of H-bond would drastically reduce the HT channels, thereby leading to significant HT congestion at OHP. On the other hand, the insufficient supply of proton to the inner interface may result in the accumulation of $OH^-$ ions, which can further increase the free energy barrier of the water dissociation thereby. The present finding highlights immense opportunities to regulate the electrochemical reaction kinetics in alkaline environment by optimizing the interfacial water distribution and the connectivity of H-bond networks. It can explain well why bringing down the electrode PZC[8,21] and/or adding the protic ionic liquids (or organic molecules) [39,41] as the electrolyte components can be sagacious strategies to improve the hydrogen electrocatalytic kinetics. The former can reduce the negative charge density on electrode surface, thereby decrease the cation concentration required to establish the EDL, and eventually improve the interfacial water distribution and H-bond networks[8,21]. The latter can construct and strengthen the

interfacial H-bond networks and serve as the role of “proton pump” to efficiently transfer the proton in the EDL[39,41].

We also evaluated the HBEs at acid and alkaline interfaces, through the calculation method introduced in the Supplementary Note 1 and Supplementary Fig. 10. Figure 2b shows that the hydrogen binding strength at acid interface is stronger than that in alkaline environment, agreeing well with the recent voltametric and spectroscopic experiments[21–23]. This demonstrates that the pH-dependent HER kinetics also cannot be described aptly by the difference in hydrogen binding strength.

**Rationalization of the H-bond network gap in alkaline EDL with the results from** in situ **SEIRAS.** To corroborate the H-bond network gap in the alkaline EDL, we have conducted *in situ* surface-enhanced IR spectroscopy (SEIRAS) measurements in attenuated total reflection (ATR) mode and compared the experimental vibration responses with the computational vibrational density of states (VDOS) of interfacial water molecules in the simulated EDLs. The ATR-SEIRAS given in the form of differential spectra usually has excellent surface enhancement effect and sensitivity within ~5-10 nm away from the electrode surface[45], thus enabling accurate detection of the EDL structures at electrochemical interfaces.

Chemically deposited Pt thin film electrode is used as the working electrode in SEIRAS. The typical cyclic voltammograms of the Pt thin film electrode in 0.1 M $HClO_4$ and NaOH solutions are shown in Supplementary Fig. 11, and both are identical to those of polycrystalline Pt in the corresponding environments[22]. The atomic force microscopy (AFM) images show that the Pt thin film electrode possesses rough surface with islands composed of Pt nanoparticles (Supplementary Fig. 12). In addition, the spectrum measured in CO-saturated 0.1 M $HClO_4$ solution exhibits only two peaks centered at 2073 $cm^{-1}$ and 1871 $cm^{-1}$ (Supplementary Fig. 13), which are assigned to the C-O stretching modes of CO adsorbed on the atop and bridge sites of Pt surface, respectively[46,47]. This indicates that the Au substrate is completely covered by the deposited Pt film and thus has negligible interference on the IR spectra measurement.

Figure 3a,b show the *in situ* SEIRA spectra of interfacial water molecules on Pt at various potentials in Ar-saturated 0.1 M NaOH and $HClO_4$ solutions, respectively. The spectra are given in the form of differential spectra with that collected at potentials close to the PZC of Pt electrode, namely, 0.9 V in alkaline and 0.5 V in acid. Using these reference spectra, we can obtain the spectral changes associated with the gradual formation of the EDL as the potential deviates from the PZC[22,48,49]. On the other hand, we have calculated the vibrational density of states (VDOSs) for the interfacial water molecules within ~6.6 Å from the Pt surface in the AIMD-simulated EDLs at alkaline and acid interfaces. As shown in Fig. 3c,d, the computational spectra possess very similar shapes to that of the experimental SEIRA spectra. Specifically, the O-H stretching peak of interfacial water displays a broader and symmetric shape in alkaline system while a more asymmetric shape extending toward the lower frequency region in acid system. In addition, it is noted that the experimental O-H stretching peak in NaOH solution can be deconvoluted into three distinct components through Gaussian fitting (Fig. 3e and Supplementary

Fig. 14a); while in $HClO_4$ solution, the O-H stretching band can only be resolved into two components (Fig. 3f and Supplementary Fig. 14b). The deconvolution of the computational VDOS of O-H stretching mode exhibits the nearly identical features (Fig. 3g,h). These consistencies not only indicate that the ATR-SEIRS signals were mainly derived from the first few layers of water molecules close to the electrode surface, but also confirm that the AIMD-simulated EDL structures reasonably represent that at the real electrochemical interfaces. Therefore, the existence of H-bond network gap at the alkaline interfaces can be convinced.

To further understand the experimental and computed vibrational spectra, the VDOS of interfacial water molecules at different distances from the electrode surface have been calculated. Figure 4a shows the schematic diagram of region division, in which the Region 2 is the gap region of water molecules and H-bond networks. As shown in Fig. 4b, the O-H stretching vibration peak of water molecules at alkaline interface exhibits a feature of first blue shift then red shift with the distance away from the electrode surface. The water molecules located in the gap region (denoted as $H_2O_{(gap)}$) have the highest O-H stretching vibration frequency, while those above the gap region (denoted as $H_2O_{(above-gap)}$) and those nearest to the electrode surface (denoted as $Na.H_2O_{(Pt)}$) have the second and lowest O-H stretching vibration frequencies, respectively. These features of theoretical spectra seem to agree well with the experimental observation that the O-H stretching spectra for water molecules at alkaline interface can be deconvoluted into three distinct components. Consequently, the high wavenumber component (green shadow), main component (yellow shadow) and low wavenumber component (blue shadow) in Fig. 3e and 3g are associated with $H_2O_{(gap)}$, $H_2O_{(above-gap)}$ and $Na.H_2O_{(Pt)}$, respectively. In acid system, the $H_2O_{(gap)}$ gives a slightly higher theoretical O-H stretching wavenumber, while the other interfacial water molecules (denoted as $H_2O_{(none-gap)}$) exhibit nearly the same O-H stretching vibration frequency (Supplementary Fig. 15), which seems to explain well why the experimenta spectra for acid system can only be deconvoluted into two distinct components (Fig. 3f and 3h). These results reveal that the $H_2O_{(gap)}$ usually has a stronger O-H stretching vibration when comparing to the adjacent water molecules, which should further suggest the relative scarcity of H-bond networks in the gap region.

To further compare the degrees of the H-bond network gap at alkaline and acid interfaces, the potential dependence of O-H stretching vibration frequencies of each type of interfacial water molecules at alkaline and acid interfaces are compared (Supplementary Fig. 16). As well as the frequencies shift due to the vibrational Stark effect[50], it is noted that the difference in the O-H stretching wavenumbers between $H_2O_{(gap)}$ and $H_2O_{(above-gap)}$ in alkaline system (~150 $cm^{-1}$) is much higher than that between $H_2O_{(gap)}$ and $H_2O_{(none-gap)}$ in acid system (~72 $cm^{-1}$), demonstrating the much more severe scarcity of H-bond networks in alkaline EDL. On the other hand, the potential-dependent proportions of the deconvoluted peak for $H_2O_{(gap)}$ in alkaline and acid environments have been analyzed. It is found that the proportion of $H_2O_{(gap)}$ molecules at alkaline interface gradually decreases with the potential decreasing (Fig. 4c), which should be due to the more serious depletion of water molecules and H-bond networks caused by the increased $Na^+$ concentration in the EDL. By contrast, the proportion of $H_2O_{(gap)}$ molecules at acid

interface not only is much higher than that at alkaline interface, but also shows negligible change with potential (Fig. 4d), which suggests that the gap of H-bond networks is almost negligible in acid system. In addition, it's encouraging that the proportions of $H_2O_{(gap)}$ (marked by red circles) derived from the computational VDOS for both alkaline and acid systems reasonably agree with that calculated from the experimental SEIRAS spectra, further convincing the simulated EDL structures and the decreased connectivity of H-bond networks in the alkaline EDL.

**Improving the connectivity of H-bond networks by OH adsorption.** Numerous recent studies have revealed that alloying Pt with Ru can significantly enhance the HOR/HER kinetics in alkaline electrolyte, which has been ascribed to the facilitated water formation/dissociation due to the increased OH/$H_2O$ adsorption on the more oxophilic Ru atoms[25,30,33]. As shown in last section, the water dissociation may not be the major cause of the decreased activity of Pt for hydrogen electrocatalytic reaction in alkaline electrolyte, while the connectivity of H-bond networks near OHP may be a dominant factor of the kinetic pH effect. Therefore, we investigate the effect of OH adsorption on the connectivity of interfacial H-bond networks, using the $Pt_3Ru(111)$ as a model surface. Figure 5a,b show the AIMD-simulated atomic structures of alkaline interfaces on $Pt_3Ru(111)$ electrodes with and without OH adsorption, and the electrode potentials are driven to values corresponding to the HOR potentials for pH=14 by inserting three $Na^+$ counter-ions, which are ~0.40 V and ~0.14 V, respectively. We consider HOR here because it has been shown the Pt-Ru alloys usually exhibit much more pronounced activity promotion for HOR[25,30]. Meanwhile, the interface on the Pt(111) electrode that contains the same number of $Na^+$ cations is also simulated for comparison (Fig. 5c). As shown in Fig. 5d, the water concentration distributions in the interfacial structures of $Pt_3Ru(111)$ electrode without OH adsorption are very similar to that of the Pt(111) electrode, both exhibiting fairly low water concentrations within the green shaded region (viz. the "gap zone" above the OHP); while for the interface on the $Pt_3Ru(111)$ electrode with OH adsorbed on Ru site, the water concentration within the green shaded region is apparently higher. The increased number of water molecules in the gap zone is also manifested by the integral water concentration distributions (Supplementary Fig. 17) and the H-bond number profiles (Fig. 5e). This suggests that the OH adsorption can significantly increase the water connectivity and improve the H-bond networks in the EDL. To further understand this phenomenon, the EDL structures of the interfaces on $Pt_3Ru(111)$ electrodes with and without OH adsorption are carefully compared. First, one can find that on $Pt_3Ru(111)$ electrode with OH adsorption, the $Na^+$ ions mainly gather around the adsorbed OH species due to the coordination interaction, rather than being more spread over the electrode surface as that on the bare $Pt_3Ru(111)$, as shown in Fig. 5a,b and Supplementary Fig. 18. The aggregation of cations around OH would increase the space for water molecules in the OHP region. On the other hand, it's noted that the coordination between $Na^+$ ions and adsorbed OH leaves more free water molecules (Supplementary Fig. 18), which possess stronger ability to form H-bond with others. These results suggest that the adsorbed OH species promote the alkaline HOR activity mainly through regulating the interfacial EDL structures.

# Conclusions

The roles of EDL structure in the kinetic pH effect of hydrogen electrocatalysis on Pt-based electrodes are understood by combining AIMD simulations and *in situ* SEIRAS spectroscopy measurements. The results suggest that neither the hydrogen adsorption strength nor the water dissociation barrier may be responsible for the greatly reduced kinetics of hydrogen electrocatalysis in alkaline solution; rather, the water distribution and the connectivity of H-bond networks in EDL play a dominating role. We also revealed an unprecedented role of the adsorbed OH in impacting the electrocatalytic activity, namely, by modulating the water connectivity and improving the H-bond networks in the EDL, rather than by facilitating the water dissociation/formation. Our findings highlight the significance of EDL microstructures in the electrocatalytic reaction kinetics and could provide new guidance for designing pH-oriented electrocatalysts. Meanwhile, this study may also offer a referential research mode for the future exploration of atomic structures of electrochemical interfaces by combining the experimental and computational spectroscopy.

# Methods

**Computations and models.** All AIMD simulations are performed using Vienna Ab initio Simulation Package (VASP), a plane-wave pseudopotential code[51-53]. The Perdew-Burke-Ernzerhof (PBE) functional within the generalized gradient approximation (GGA) is applied to evaluate the exchange and correlation energies[54]. The wave functions are expanded up to a cutoff energy of 400 eV and the First order Methfessel-Paxton scheme with a smearing width of 0.2 eV is employed. The van der Waals interaction is considered through the semi-empirical D3 dispersion correction scheme of Grimme[55]. Non-spin polarization is included in all simulations, because it has almost no effect on the overall energies. The timestep is set as 1.0 fs, and only the gamma point of the Brillouin zone with no consideration of symmetry is used. Nose-Hoover thermostat is applied to keep the temperature of canonical ensemble (NVT) at 298 K.

The Pt(111)/water interface is modeled by adding 60 water molecules above a four-layer 4´4 orthogonal Pt(111) slab with a surface area of 1.10 $nm^2$. The thickness of water film and vacuum layer are ~1.6 nm and ~2.4 nm, respectively, and the size of the whole simulation box is ~4.9 nm along the z-axis. To fully equilibrate the hydrogen bond networks of water layer and reduce the AIMD simulation time, we firstly perform a 250 ps classical MD simulation with reactive force field at 298 K by using the Largescale Atomic/Molecular Massively Parallel Simulator (LAMMPS) with user package of Reax/C[56,57]. The Pt-O-H reactive force field developed by Shin et al. is applied to describe the interaction between water and metal surface[58]. The pre-equilibrated Pt(111)/water interface given by the classic MD simulations is used as the initial configuration to perform AIMD simulations. All AIMD trajectories are sampled for runtimes of up to 15-25 ps, to ensure that the interface systems are well equilibrated, and in which, the snapshots in the last 10 ps are implied for statistical analyzes.

According to $U_{SHE} = \emptyset - \emptyset_{SHE}$, where $\emptyset$ is the work function of interface system and $\emptyset_{SHE}$

is the work function of the standard hydrogen electrode (SHE, 4.44 V)[59], the potential of zero charge (PZC) of Pt(111)/water interface is calculated as 0.21 V, being well in line with the experimental measurements and other MD simulations[60,61]. The vibrational density of states (VDOS) of interfacial water molecules (within ~6.6 Å away from Pt surface) were calculated by the Fourier transformation of the velocity auto-correlation functions (VACF) in the AIMD trajectories.

To simulate the acid and alkaline environments, we explicitly insert hydronium ion ($H_3O^+$) and Na ion ($Na^+$) into water film, respectively. These ions are initially putted at ~3-4 Å away from the Pt(111) surface to model the compact Helmholtz layer. The Gouy-Chapman diffusion layer is omitted when considering the relatively high ion concentration of electrolytes in experiments. The co-ions are also neglected because that the electrode surfaces should be highly charged at HER potentials and the co-ions should be repelled away from the Helmholtz plane. Meanwhile, since the whole system is kept charge neutral, the same number of electrons as that of inserted ions will be introduced into the metal surface to tune the Fermi level. Thus, we can vary the number of inserted ions to control the surface charge density and then the electrode potential to reach the potential range of hydrogen evolution. The electrode potentials with respect to that of the reversible hydrogen electrode are estimated according to

$$U_{RHE} = \frac{\emptyset - \emptyset_{SHE}}{e} + 0.059 * \mathrm{pH}.$$

In addition, the hydrogen adsorption intermediate ($H_{ad}$) is taken into account to describe the surface state of Pt(111) electrode under the hydrogen evolution potential as truthfully as possible, and the coverages are set as 0.88 ML (defined per surface atom) and 0.63 ML for acid and alkaline systems respectively, according to previous experimental results[62,63]. The peculiar advantage of our theoretical model lies in that the electrode potential, the properties and ion concentration of acid/alkaline EDL and the species adsorbed on the electrode surface are approximately self-consistent, which will provide a reasonable description of the pH-dependent reaction kinetics.

The slow-growth approach[64-66], within the constrained molecular dynamics (CMD) framework, is utilized to calculate the free energy profile of the $H_{ad}$ formation process (Volmer step), namely the $H_3O^+$ dissociation ($H_3O^+ + e^- \leftrightarrow *H + H_2O$) in acid solution and $H_2O$ dissociation ($H_2O + e^- \leftrightarrow *H + OH^-$) in alkaline solution. The increment of 0.0008 Å/fs to CV is set to drive the chemical reactions. Three independent simulations are performed for each reaction to ensure the accuracy and reliability of the free energy barrier results. In addition, all CMD simulations are carried out under constant charge condition, meaning that the work functions will change along the reaction pathway. To gain the constant potential results and compare with experiments, the correction procedure proposed by Chan and Nørskov is employed to remove any artifacts due to work function changes during the simulation[67,68]. The detailed principles of slow-growth approach and constant potential correction can be found in the Supplementary Notes 2 and 3.

**Preparation of Pt thin film electrode.** The Pt thin film working electrode was prepared by a typical two-step deposition method[22,69], involving the chemical deposition of an Au thin film on the hemispheric Si prism followed by the galvanostatic electrodeposition of a Pt thin film on the Au substrate. Before the chemical deposition of Au, the Si prism was first polished gradually using 1.0, 0.3, 0.05 μm $Al_2O_3$ powder for about 30 min until the surface becomes totally hydrophobic, and then sonicated and rinsed several times with acetone/ethanol (Sinopharm Chemical Reagent Co., Ltd., AR) mixed solution (volume ratio V:V=1:1) and double deionized-distilled water (ULUPURE, 18.2 MW). After that, the hydrophobic and clean Si prism was undergone hydroxylation treatment with Piranha solution (the volume ratio between concentrated $H_2SO_4$ and 30% $H_2O_2$ is 1:1) for 20 min and then sonicated with distilled water for several times. The IR reflection plane of the Si prism was then dried by Ar (UHP grade) flow and treated by 40% $NH_4F$ (Sinopharm Chemical Reagent Co., Ltd., AR) for 2 min to make the surface terminated with hydrogen. The thin Au film was then deposited on the hydrogen-terminated surface by immediately immersing this plane into a mixture of 9.2 mL Au plating solution and 124 μL 50% HF solution (Sinopharm Chemical Reagent Co., Ltd., AR) at 55-60℃ for 6 min. A voltmeter was used to measure the conductivity of the Au film, showing an ohmic resistance lower than 10 W. The Au-coated prism was mounted into a homemade spectroelectrochemical cell as the working electrode, a calibrated saturated calomel electrode (SCE) was assembled near the working electrode via a Luggin capillary as the reference electrode, and a Pt mesh with a size of 0.8 cm ´ 1.0 cm was used as the counter electrode. The Au film was electrochemically cleaned with cyclic voltammetry between 0.0 and 1.4 V (vs SCE) with a scan rate of 50 mV $s^{-1}$ in the Ar-saturated 0.1 M $HClO_4$ (KESHI, GR) solution until a repeatable cyclic voltammetry curve was obtained. After rinsing with sufficient water, electrodeposition of Pt thin film was carried out in an Ar-saturated solution of 4 mM $H_2PtCl_6$ (Kunming Sino-Platinum Co., Ltd, >98%) + 0.7 M $Na_2HPO_4$ (Aladdin Chemicals, GR) at a current density of -0.75 mA $cm^{-2}$ for 900 s followed by -0.4 mA $cm^{-2}$ for 480 s. The prepared Pt thin film was carefully washed with distilled water several times and used immediately.

***In situ* SEIRAS Experiments.** To conduct SEIRAS measurements, a Hg/HgO electrode and a homemade RHE were used as the reference electrodes in 0.1 M NaOH (Aladdin Chemicals, 99.9%) and 0.1 M $HClO_4$ solutions, respectively. A FTIR spectrometer equipped with liquid nitrogen-cooled mercury cadmium telluride (MCT) detector was used for the SEIRAS measurements and operated at a resolution of 8 $cm^{-1}$. Unpolarized infrared radiation from an Elema source was focused at the reflection plane with an incident angle of ~60°, and the totally reflected radiation was detected. All spectra in this work were shown in the absorbance ($-\log(R/R_0)$), where R and $R_0$ represents the sample and reference spectra, respectively.

**Electrochemical Measurements.** In all electrochemical and spectroscopic measurements, an PARSTAT electrochemical workstation (versaSTAT 3F) was used. All electrode potentials have been converted to the RHE scale. Before *in situ* ATR-SEIRAS measurements, the prepared Pt thin film working electrode was cycled in the corresponding electrolyte (Ar-saturated 0.1 M $HClO_4$ or 0.1 M NaOH) between 0.02 V and 1.2 V at a scanning rate of 100 mV $s^{-1}$ for two cycles to get a clean surface. Then the cyclic voltammetry curves in acid and alkaline solutions were recorded at 10 mV $s^{-1}$. To collect the IR spectra, the Pt working

electrode was initially kept at 1.2 V for 10 s, and then the potential was linearly swept from 1.2 V to -0.05 V at a scanning rate of 5 mV $s^{-1}$, during which the IR spectra were collected using the rapid-scan mode of OPUS software. Each spectrum was co-added by 44 single spectra with a resolution of 8 $cm^{-1}$ and spanned a potential window of 50 mV.

### Data availability

The data that support the findings of this study are available within the article and its Supplementary Information files or from the corresponding author upon reasonable request.

## Declarations

## Declarations

### Competing interests

The authors declare no competing interests.

## Author contributions

S.C. supervised the project. P.L. and S.C. conceived the idea and designed the experiments. P.L. performed the AIMD simulations. Y.J. performed the electrochemical and spectroscopic measurements under the guidance of S.C. and W.C.. P.L., Y.J., Y.H., Y.M., Y.L, and S.C. analyzed the data. P.L., Y.J. and S.C. wrote the manuscript. All authors discussed and commented on the manuscript.

## Acknowledgements

The authors gratefully acknowledge the financial support from the National Natural Science Foundation of China (Grant Nos. 21832004 and 21673163). Generous grants of computer time at the Supercomputing Center of Wuhan University are also gratefully acknowledged.

## References

1. Hoffert, M. I. et al. Advanced technology paths to global climate stability: energy for a greenhouse planet. Science **298**, 981–987 (2002).
2. Crabtree, G. W., Dresselhaus, M. S. & Buchanan, M. V. The hydrogen economy. Phys. Today **57**, 39–44 (2004).
3. Chow, J., Kopp, R. J. & Portney, P. R. Energy resources and global development. Science **302**, 1528–1531 (2003).
4. Turner, J. A. Sustainable hydrogen production. Science **305**, 972–974 (2014).

5. Tafel, J. (1906). Kathodenpotential und elektrolytische Reduktion in schwefelsaurer Lösung. *Angew. Phys. Chem.* **12**, 112–122 (1906).
6. Frumkin, A. Hydrogen overvoltage. Discuss. Faraday Soc. **1**, 57–67 (1947).
7. Inzelt, G. Milestones of the development of kinetics of electrode reactions. J. Solid State Electrochem. **15**, 1373–1389 (2011).
8. Huang, J., Li, P. & Chen, S. Quantitative understanding of the sluggish kinetics of hydrogen reactions in alkaline media based on a microscopic Hamiltonian model for the Volmer step. J. Phys. Chem. C, **123**, 17325–17334 (2019).
9. Sheng, W., Gasteiger, H. A. & Shao-Horn, Y. Hydrogen oxidation and evolution reaction kinetics on platinum: acid vs alkaline electrolytes. J. Electrochem. Soc. **157**, B1529–B1536 (2010).
10. Subbaraman, R. et al. Enhancing hydrogen evolution activity in water splitting by tailoring $Li^+$-$Ni(OH)_2$-Pt interfaces. Science **334**, 1256–1260 (2011).
11. Durst, J., Siebel, A., Simon, C., Hasché, F., Herranz, J. & Gasteiger, H. A. New insights into the electrochemical hydrogen oxidation and evolution reaction mechanism. Energy Environ. Sci. **7**, 2255–2260 (2014).
12. Zheng, Y., Jiao, Y., Vasileff, A. & Qiao, S. Z. The hydrogen evolution reaction in alkaline solution: from theory, single crystal models, to practical electrocatalysts. Angew. Chem. Int. Ed. **57**, 7568–7579 (2018).
13. Strmcnik, D., Lopes, P. P., Genorio, B., Stamenkovic, V. R. & Markovic, N. M. Design principles for hydrogen evolution reaction catalyst materials. Nano Energy **29**, 29–36 (2016).
14. Sheng, W., Zhuang, Z., Gao, M., Zheng, J., Chen, J. G. & Yan, Y. (2015). Correlating hydrogen oxidation and evolution activity on platinum at different pH with measured hydrogen binding energy. *Nat. Commun.* **6**, 1-6 (2015).
15. Zheng, J., Sheng, W., Zhuang, Z., Xu, B. & Yan, Y. (2016). Universal dependence of hydrogen oxidation and evolution reaction activity of platinum-group metals on pH and hydrogen binding energy. *Sci. Adv.* **2**, e1501602 (2016).
16. Giles, S. A., Wilson, J. C., Nash, J., Xu, B., Vlachos, D. G. & Yan, Y. Recent advances in understanding the pH dependence of the hydrogen oxidation and evolution reactions. J. Catal. **367**, 328–331 (2018).
17. Zheng, J., Nash, J., Xu, B. & Yan, Y. Perspective—towards establishing apparent hydrogen binding energy as the descriptor for hydrogen oxidation/evolution reactions. J. Electrochem. Soc. **165**, H27 (2018).
18. Cheng, T., Wang, L., Merinov, B. V. & Goddard III, W. A. Explanation of dramatic pH-dependence of hydrogen binding on noble metal electrode: Greatly weakened water adsorption at high pH. J. Am. Chem. Soc. **140**, 7787–7790 (2018).
19. Chen, X., McCrum, I. T., Schwarz, K. A., Janik, M. J. & Koper, M. T. Co-adsorption of cations as the cause of the apparent pH dependence of hydrogen adsorption on a stepped platinum single-crystal

electrode. *Angew. Chem. Int. Ed.* 2017, 56, 15025–15029 (2017).

20. Janik, M. J., McCrum, I. T. & Koper, M. T. On the presence of surface bound hydroxyl species on polycrystalline Pt electrodes in the "hydrogen potential region" (0-0.4 V-RHE). J. Catal. **367**, 332–337 (2018).
21. Ledezma-Yanez, I., Wallace, W. D. Z., Sebastián-Pascual, P., Climent, V., Feliu, J. M. & Koper, M. T. Interfacial water reorganization as a pH-dependent descriptor of the hydrogen evolution rate on platinum electrodes. Nat. Energy **2**, 1–7 (2017).
22. Zhu, S., Qin, X., Yao, Y. & Shao, M. pH-dependent hydrogen and water binding energies on platinum surfaces as directly probed through surface-enhanced infrared absorption spectroscopy. J. Am. Chem. Soc. **142**, 8748–8754 (2020).
23. Wang, Y. H. et al. Spectroscopic verification of adsorbed hydroxy intermediates in the bifunctional mechanism of the hydrogen oxidation reaction. Angew. Chem. Int. Ed. **133**, 5772–5775 (2021).
24. Danilovic, N., Subbaraman, R., Strmcnik, D., Stamenkovic, V. & Markovic, N. Electrocatalysis of the HER in acid and alkaline media. J. Serb. Chem. Soc. **78**, 2007–2015 (2013).
25. Strmcnik, D. et al. Improving the hydrogen oxidation reaction rate by promotion of hydroxyl adsorption. Nat. Chem. **5**, 300–306 (2013).
26. Danilovic, N., Subbaraman, R., Strmcnik, D., Chang, K. C., Paulikas, A. P., Stamenkovic, V. R. & Markovic, N. M. Enhancing the alkaline hydrogen evolution reaction activity through the bifunctionality of $Ni(OH)_2$/metal catalysts. Angew. Chem. Int. Ed. **124**, 12663–12666 (2012).
27. Subbaraman, R. et al. Trends in activity for the water electrolyser reactions on 3d M (Ni, Co, Fe, Mn) hydr(oxy)oxide catalysts. Nat. Mater. **11**, 550–557 (2012).
28. Dinh, C. T. et al. Multi-site electrocatalysts for hydrogen evolution in neutral media by destabilization of water molecules. Nat. Energy **4**, 107–114 (2019).
29. Men, Y., Li, P., Zhou, J., Chen, S. & Luo, W. Trends in alkaline hydrogen evolution activity on cobalt phosphide electrocatalysts doped with transition metals. Cell Rep. Phys. Sci. **1**, 100136 (2020).
30. Wang, Y. et al. Pt–Ru catalyzed hydrogen oxidation in alkaline media: oxophilic effect or electronic effect? Energy Environ. Sci. **8**, 177–181 (2015).
31. Intikhab, S., Snyder, J. D. & Tang, M. H. Adsorbed hydroxide does not participate in the Volmer step of alkaline hydrogen electrocatalysis. ACS Catal. **7**, 8314–8319 (2017).
32. Rebollar, L., Intikhab, S., Snyder, J. D. & Tang, M. H. Determining the viability of hydroxide-mediated bifunctional HER/HOR mechanisms through single-crystal voltammetry and microkinetic modeling. J. Electrochem. Soc. **165**, J3209 (2018).
33. McCrum, I. T. & Koper, M. T. The role of adsorbed hydroxide in hydrogen evolution reaction kinetics on modified platinum. Nat. Energy **5**, 891–899 (2020).
34. Li, J. et al. Experimental proof of the bifunctional mechanism for the hydrogen oxidation in alkaline media. Angew. Chem. Int. Ed. **56**, 15594–15598 (2017).

35. Rebollar, L. et al. “Beyond adsorption” descriptors in hydrogen electrocatalysis. ACS Catal. **10**, 14747–14762 (2020).
36. Sarabia, F. J., Sebastián-Pascual, P., Koper, M. T., Climent, V. & Feliu, J. M. Effect of the interfacial water structure on the hydrogen evolution reaction on Pt (111) modified with different nickel hydroxide coverages in alkaline media. ACS Appl. Mater. Interfaces **11**, 613–623 (2018).
37. Ramaswamy, N., Ghoshal, S., Bates, M. K., Jia, Q., Li, J. & Mukerjee, S. Hydrogen oxidation reaction in alkaline media: Relationship between electrocatalysis and electrochemical double-layer structure. Nano Energy **41**, 765–771 (2017).
38. Shen, L. F. et al. Interfacial structure of water as a new descriptor of the hydrogen evolution reaction. Angew. Chem. Int. Ed. **132**, 22583–22588 (2020).
39. Wang, T. et al. Enhancing oxygen reduction electrocatalysis by tuning interfacial hydrogen bonds. Nat. Catal. **4**, 753–762 (2021).
40. Berg, N., Bergwinkl, S., Nuernberger, P., Horinek, D., & Gschwind, R. M. Extended hydrogen bond networks for effective proton-coupled electron transfer (PCET) reactions: the unexpected role of thiophenol and its acidic channel in photocatalytic hydroamidations. J. Am. Chem. Soc. **143**, 724–735 (2021).
41. Lan, Y. Q. et al. Implanting numerous hydrogen-bonding networks in Cu-porphyrin based nanosheet to boost $CH_4$ selectivity in neutral media $CO_2$ electroreduction. Angew. Chem. Int. Ed. **60**, 2–9 (2021).
42. Liu, Y., Kawaguchi, T., Pierce, M. S., Komanicky, V. & You, H. Layering and ordering in electrochemical double layers. J. Phys. Chem. Lett. **9**, 1265–1271 (2018).
43. Strmcnik, D. et al. Effects of $Li^+$, $K^+$, and $Ba^{2+}$ cations on the ORR at model and high surface area Pt and Au surfaces in alkaline solutions. J. Phys. Chem. Lett. **2**, 2733–2736 (2011).
44. Dubouis, N., Serva, A., Salager, E., Deschamps, M., Salanne, M. & Grimaud, A. The fate of water at the electrochemical interfaces: electrochemical behavior of free water versus coordinating water. J. Phys. Chem. Lett. **9**, 6683–6688 (2018).
45. Dunwell, M., Yan, Y. & Xu, B. A surface-enhanced infrared absorption spectroscopic study of pH dependent water adsorption on Au. Sur. Sci. **650**, 51–56 (2016).
46. Yamakata, A. & Osawa, M. Dynamics of double-layer restructuring on a platinum electrode covered by CO: laser-induced potential transient measurement. J. Phys. Chem. C **112**, 11427–11432 (2008).
47. Osawa, M., Tsushima, M., Mogami, H., Samjeske, G. & Yamakata, A. Structure of water at the electrified platinum– water interface: A study by surface-enhanced infrared absorption spectroscopy. J. Phys. Chem. C **112**, 4248–4256 (2008).
48. Zhu, S. et al. The role of ruthenium in improving the kinetics of hydrogen oxidation and evolution reactions of platinum. Nat. Catal. **4**, 711–718 (2021).
49. Huang, B. et al. Cation- and pH-Dependent Hydrogen Evolution and Oxidation Reaction Kinetics. JACS Au **1**, 1674–1687 (2021).

50. Lambert, D. K. Vibrational Stark effect of adsorbates at electrochemical interfaces. Electrochim. Acta **41**, 623–630 (1996).
51. Kresse, G. & Hafner, J. Ab initio molecular dynamics for liquid metals. Phys. Rev. B **47**, 558–561 (1993).
52. Kresse, G. & Hafner, J. Ab initio molecular-dynamics simulation of the liquid-metal–amorphous-semiconductor transition in germanium. Phys. Rev. B **49**, 14251–14269 (1994).
53. Kresse, G. & Furthmüller, J. Efficiency of ab-initio total energy calculations for metals and semiconductors using a plane-wave basis set. Comput. Mater. Sci. **6**, 15–50 (1996).
54. Perdew, J. P., Chevary, J. A., Vosko, S. H., Jackson, K. A., Pederson, M. R., Singh, D. J. & Fiolhais, C. Atoms, molecules, solids, and surfaces: Applications of the generalized gradient approximation for exchange and correlation. Phys. Rev. B **46**, 6671–6687 (1992).
55. Grimme, S., Antony, J., Ehrlich, S. & Krieg, H. A consistent and accurate ab initio parametrization of density functional dispersion correction (DFT-D) for the 94 elements H-Pu. J. Chem. Phys. **132**, 154104 (2010).
56. Plimpton, S. Fast parallel algorithms for short-range molecular dynamics. J. Comput. Phys. **117**, 1–19 (1995).
57. Aktulga, H. M., Fogarty, J. C., Pandit, S. A. & Grama, A. Y. Parallel reactive molecular dynamics: Numerical methods and algorithmic techniques. Parallel Comput. **38**, 245–259 (2012).
58. Shin, Y. K., Gai, L., Raman, S. & Van Duin, A. C. Development of a ReaxFF reactive force field for the Pt–Ni alloy catalyst. J. Phys. Chem. A **120**, 8044–8055 (2016).
59. Trasatti, S. The absolute electrode potential: an explanatory note (Recommendations 1986). Pure Appl. Chem. **58**, 955–966 (1986).
60. Le, J., Iannuzzi, M., Cuesta, A. & Cheng, J. Determining potentials of zero charge of metal electrodes versus the standard hydrogen electrode from density-functional-theory-based molecular dynamics. Phys. Rev. Lett. **119**, 016801 (2017).
61. Li, P., Huang, J., Hu, Y. & Chen, S. Establishment of the potential of zero charge of metals in aqueous solutions: different faces of water revealed by ab initio molecular dynamics simulations. J. Phys. Chem. C, **125**, 3972–3979 (2021).
62. Markovic, N. M., Gasteiger, H. A. & Ross, P. N. Oxygen reduction on platinum low-index single-crystal surfaces in alkaline solution: rotating ring disk$_{Pt(hkl)}$ studies. J. Phys. Chem. **100**, 6715–6721 (1996).
63. Marković, N. M., Grgur, B. N. & Ross, P. N. Temperature-dependent hydrogen electrochemistry on platinum low-index single-crystal surfaces in acid solutions. J. Phys. Chem. B **101**, 5405–5413 (1997).
64. Woo, T. K., Margl, P. M., Blöchl, P. E. & Ziegler, T. A combined Car–Parrinello QM/MM implementation for ab initio molecular dynamics simulations of extended systems: application to transition metal catalysis. J. Phys. Chem. B **101**, 7877–7880 (1997).

65. Jarzynski, C. Nonequilibrium equality for free energy differences. Phys. Rev. Lett. **78**, 2690–2693 (1997).
66. Oberhofer, H., Dellago, C. & Geissler, P. L. Biased sampling of nonequilibrium trajectories: Can fast switching simulations outperform conventional free energy calculation methods? J. Phys. Chem. B **109**, 6902–6915 (2005).
67. Chan, K. & Nørskov, J. K. Electrochemical barriers made simple. J. Phys. Chem. Lett. **6**, 2663–2668 (2015).
68. Chan, K. & Nørskov, J. K. Potential dependence of electrochemical barriers from ab initio calculations. J. Phys. Chem. Lett. **7**, 1686–1690 (2016).
69. Yan, Y. G., Li, Q. X., Huo, S. J., Ma, M., Cai, W. B. & Osawa, M. Ubiquitous strategy for probing ATR surface-enhanced infrared absorption at platinum group metal–electrolyte interfaces. J. Phys. Chem. B **109**, 7900–7906 (2005).

# Figures

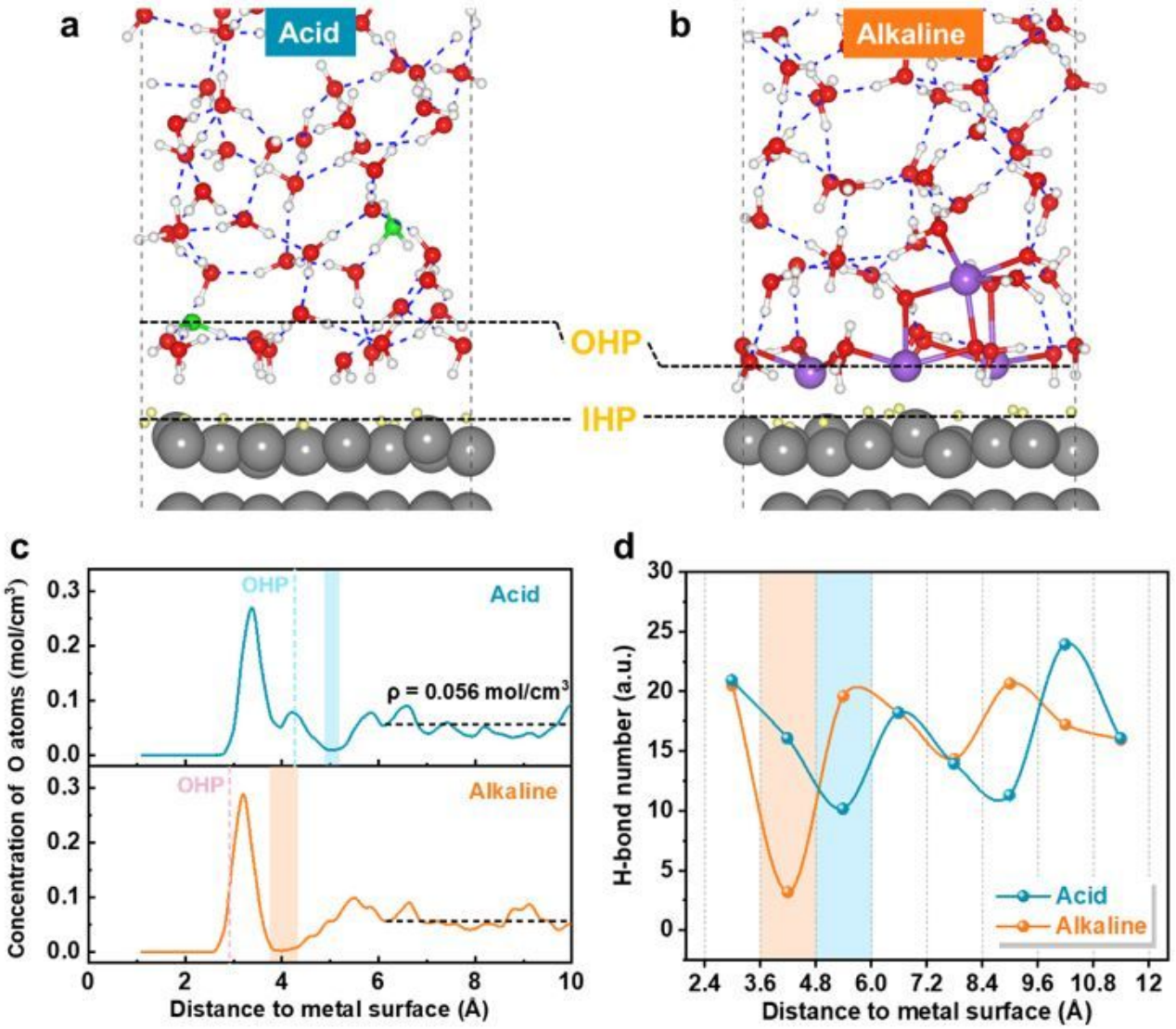


## Figure 1

**EDL structures at acid and alkaline interfaces. a**,**b**, Representative snapshots of the EDL structures under hydrogen evolution potential on the Pt(111) electrode surface for acid system (**a**) and alkaline system (**b**). The Pt, O, H, $H_3O^+$, $Na^+$ and $H_{ad}$ are colored in gray, red, white, green, purple and yellow, respectively. The blue dashed lines represent the hydrogen bonds. **c**, Concentration distribution profiles of O atoms in water molecules. The vertical dashed lines represent the OHP. The horizontal black dashed lines represent the bulk water concentration (0.056 mol/cm$^3$). **d**, Statistic distribution of the H-bond number along the surface normal direction.

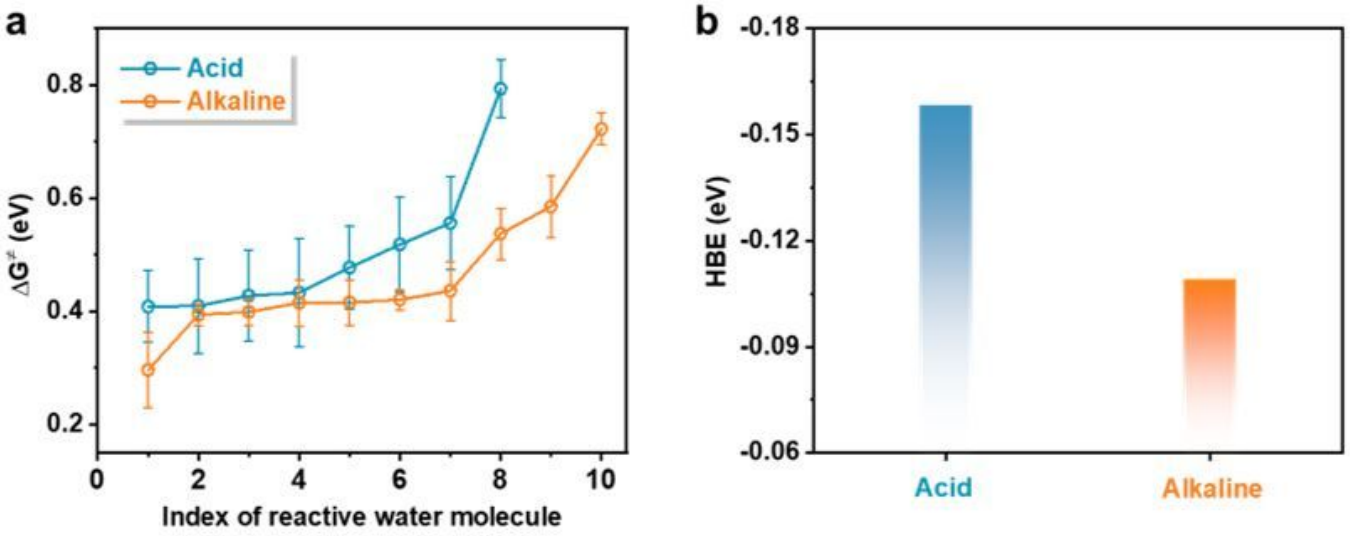


Figure 2

**Comparison of Volmer barriers and HBEs at acid and alkaline interfaces. a**, The calculated free energy barrier $\Delta G^1$ of the individual Volmer reaction for the closest water molecules at acid and alkaline interfaces. **b**, The calculated HBEs at acid and alkaline interfaces.

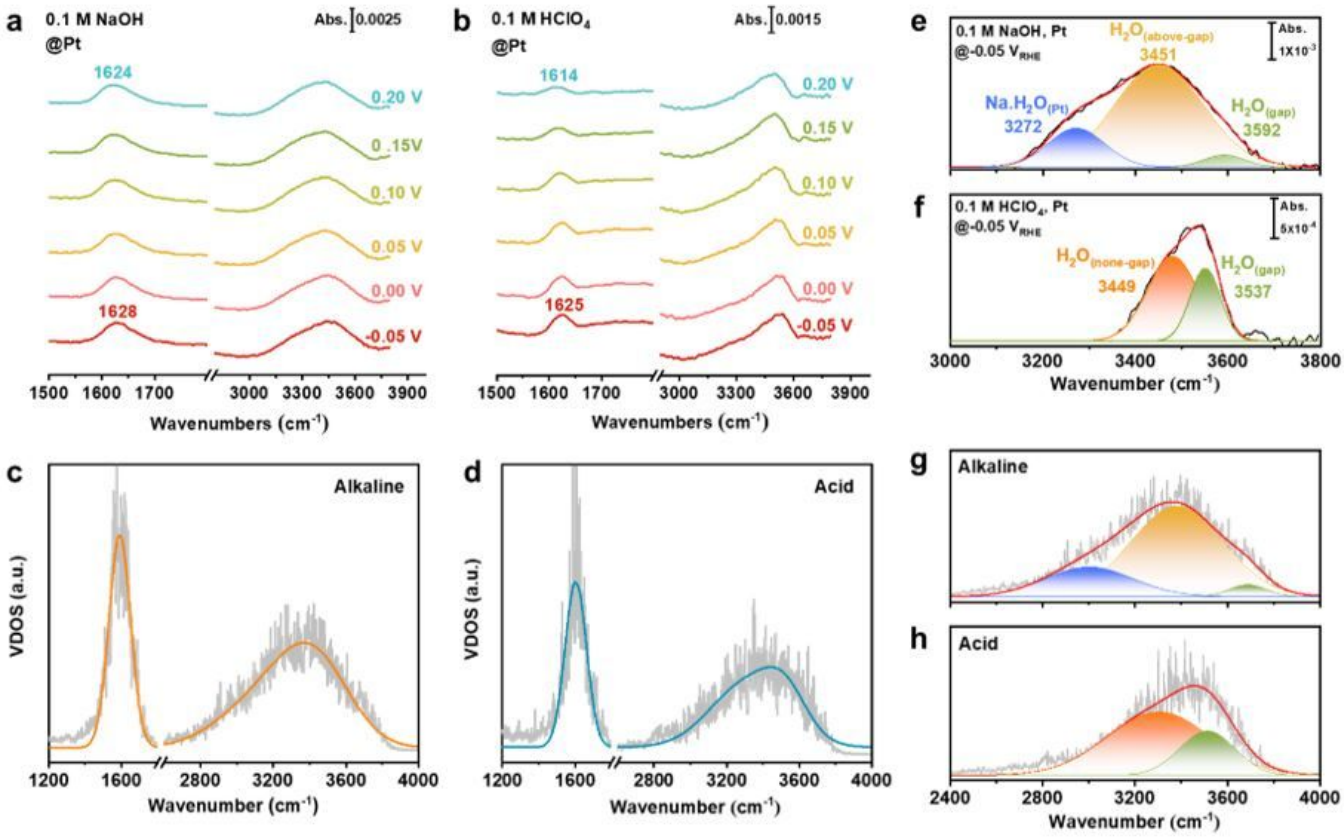


Figure 3

**IR spectra. a**,**b**, *In situ* SEIRAS spectra recorded at potentials from 0.20 V to -0.05 V for Pt electrode in Ar-saturated solutions of 0.1 M NaOH (**a**) and 0.1 M $HClO_4$ (**b**), respectively. Spectra subtracted by the reference spectrum taken at 0.9 V and 0.5 V for alkaline and acid systems, respectively. **c**,**d**, The computational VDOS of interfacial water molecules within ~6.6 Å from the electrode surface at alkaline (**c**) and acid (**d**) interfaces, respectively. **e**,**f**, Deconvolution of the experimental O-H stretching vibration peak at -0.05 V in NaOH (**e**) and $HClO_4$ (**f**) solutions. **g**,**h**, Deconvolution of the computational O-H stretching vibration peak at alkaline (**g**) and acid (**h**) interfaces.

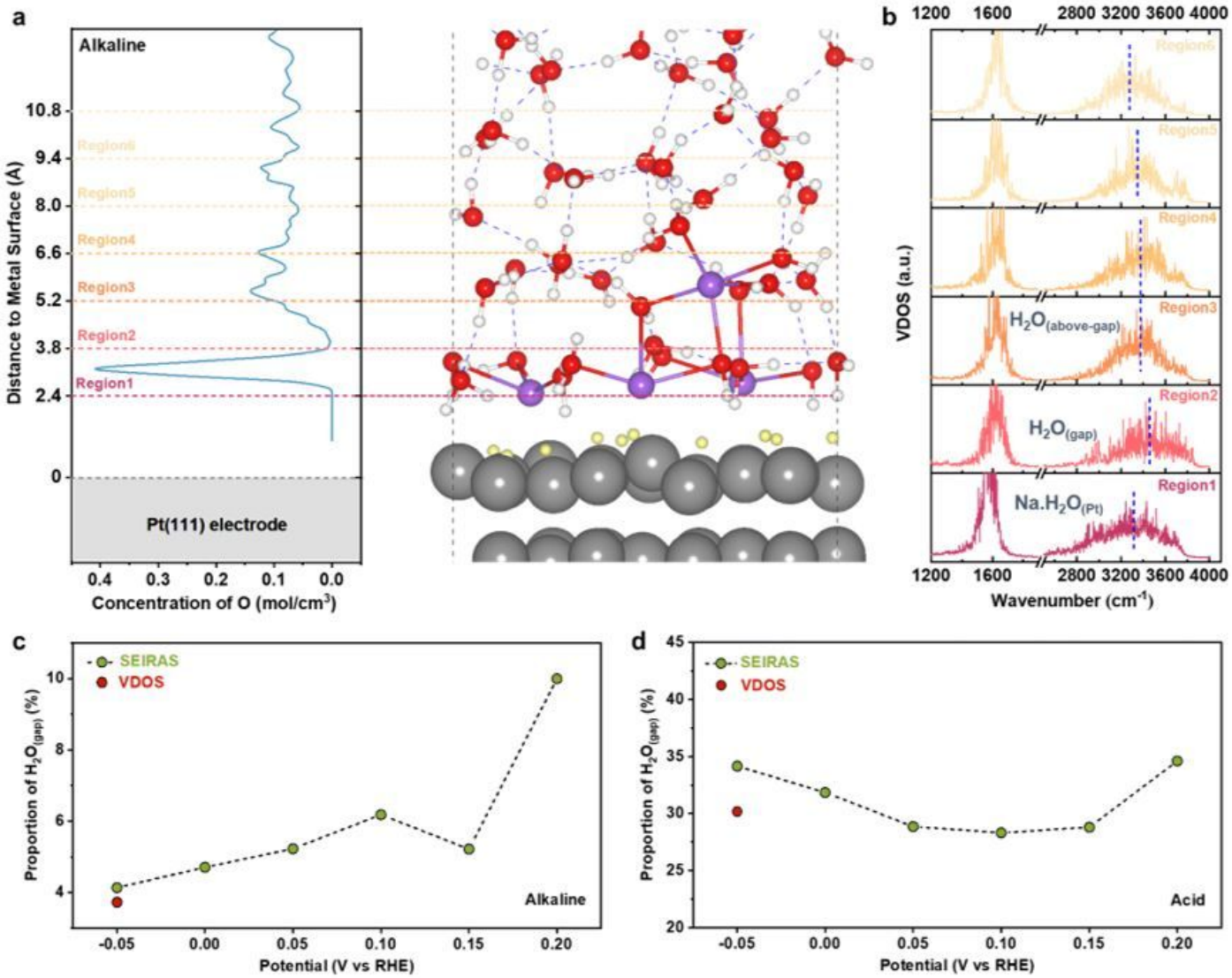


## Figure 4

**Spectroscopic analysis of different interfacial water molecules. a**, Schematic diagram of region division for the alkaline system. Region 2 represents the gap of H-bond networks. **b**, The computational VDOS of the water molecules at various distances from the electrode surface under alkaline condition. **c**,**d**, Potential-dependent proportion of $H_2O_{(gap)}$ from *in situ* SEIRAS spectra at alkaline (**c**) and acid (**d**) interfaces, respectively. The isolated red circles are that calculated from the VDOS.

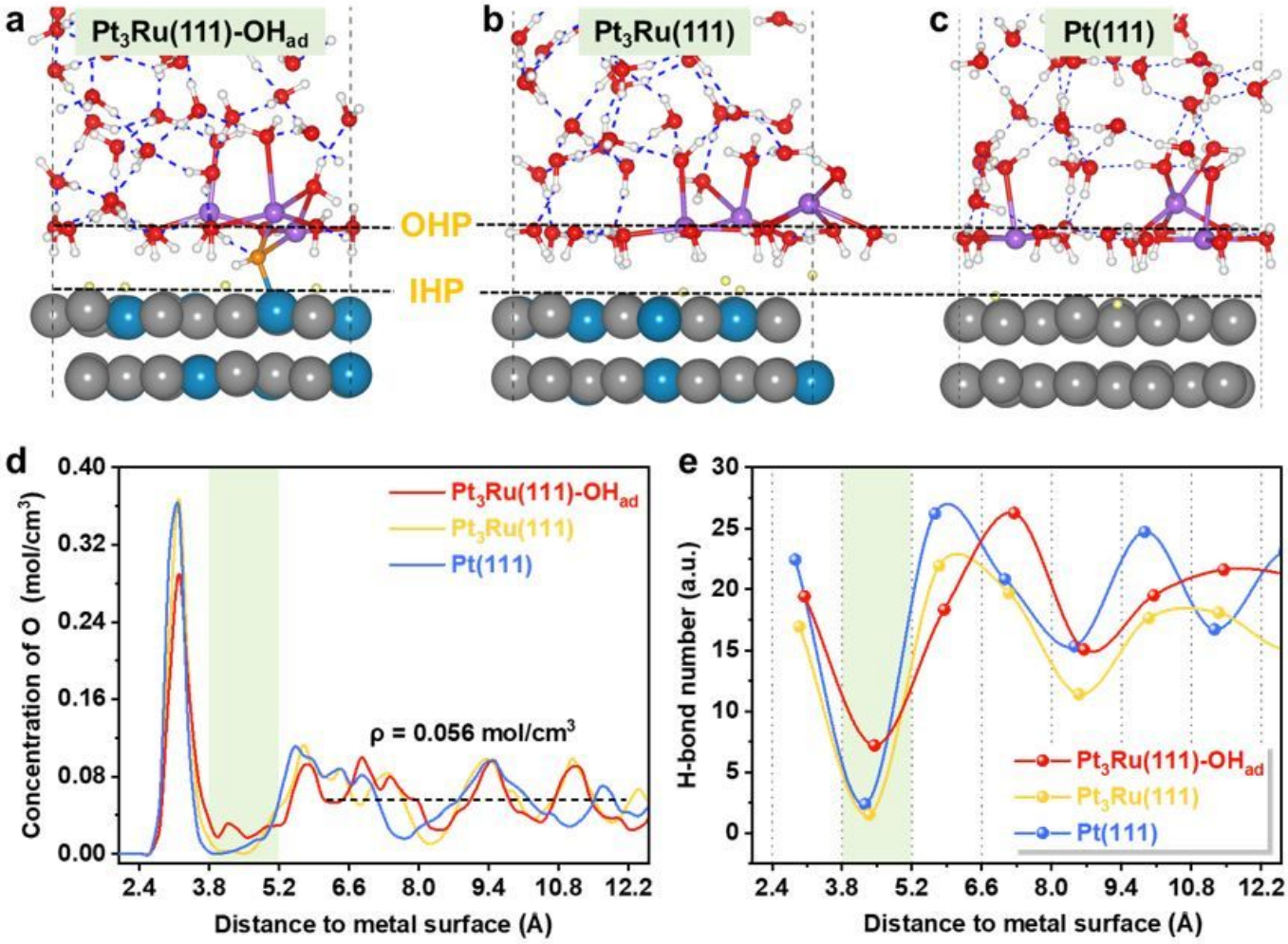


**Figure 5**

**Improvement of the connectivity of interfacial H-bond networks by $OH_{ad}$. a-c,** Representative snapshots of the AIMD-simulated interface structures on $Pt_3Ru(111)$ electrode with (**a**) and without (**b**) OH adsorption and that on Pt(111) electrode (**c**). The coverage of $H_{ad}$ is set 0.25 ML (defined per surface Pt atom). The Pt, Ru, O, H, $Na^+$, $OH_{ad}$ and $H_{ad}$ are colored in gray, tibetan cyanine, red, white, purple, orange and yellow, respectively. **d,** The concentration distribution profiles of O atoms of water. **e,** Statistic distribution of H-bond number along the surface normal direction.

# Supplementary Files

This is a list of supplementary files associated with this preprint. Click to download.

- SupplementaryInformation.pdf